

Design of a Soft Upper Body Robot for Physical Human-Robot Interaction

Alexander Alspach, Joohyung Kim, and Katsu Yamane

Abstract—To physically interact with children, a robot should be safe and durable. We have developed a small toy sized robot with a soft skin that is robust to playful physical interaction. The upper body, including the arms, pelvis, chest and back has soft, 3D printed air-filled modules connected to pressure sensors to sense contact and provide protection to the child and robot while interacting. These soft skin modules cover the underlying actuators and the rigid 3D printed frame with printed bearings. In this paper, we present the design process of these modules and demonstrate their efficacy by implementing a “grab and move” user interface for posing the robot link by link.

I. INTRODUCTION

As robotic systems become cheaper, more reliable and more capable, their prevalence in our everyday environment continues to increase. Robots can be found providing interactive guidance or entertainment in stores and amusement parks, and in more dynamic settings like homes, schools, hospitals and the workplace, where they teach, provide therapy or lend an extra set of hands [1]–[7]. In these scenarios, robots and humans often work in close proximity, physically interacting with one another.

Where physical human-robot interaction is expected, the robot’s joints and body parts should be compliant and yielding to avoid injury and damage. While passive compliance can be realized using deformable materials, active compliance uses sensor data to react to both expected and unexpected contacts. A soft robot that senses contact integrates these approaches to ensure human safety during physical interaction.

In nursing homes, PARO [6], a furry seal robot, responds to being held and pet and helps keep our older generations socially active and engaged. Another therapeutic robot, Huggable [8], features a sensorized silicone skin that covers its underlying mechanics. While these robots respond to touch in various ways, their motions are limited. More heavily actuated systems, like humanoids Macket [9] and CB² [10], have the ability to move much more and employ soft, sensorized skins to ensure human safety during physical interaction. These robot skins can sense contact in high resolution but involve complicated electronics. On the other hand, Baxter [7], a robot with hard plastic shells, works safely alongside humans by using series elastic actuators to sense contacts. This sensing method also allows users to teach the robot new tasks in a natural way by guiding its

Alexander Alspach, Joohyung Kim, and Katsu Yamane are with Disney Research, Pittsburgh, 4720 Forbes Ave., Suite 110, Pittsburgh, PA 15213, USA {alex.alspach, joohyung.kim, kyamane}@disneyresearch.com



Fig. 1. Developed robotic upper body system with 3D printed soft skin modules. Our goal is the realization of a robot that can safely and playfully physically interact with children.

limbs and end effectors, thereby sharing their workload with the robot.

Our goal is the realization of a small toy-sized humanoid robot which is soft, safe and robust during playful physical interaction with children. This robot’s locomotive style and other motions, as well as its physical form and kinematic structure, are modeled after a given animated character. Compliant joints and soft links with integrated sensors are used for safety and interactivity.

To reduce the time and effort necessary to build a full body sensory skin, we have developed a 3D printed air-filled, soft skin module [11]. This module, when connected to a pressure sensor and simple electronics, provides contact force feedback and passively absorbs impacts. In this paper, we develop a general methodology for designing soft skin for robots with size and shape constraints. We apply this to the upper body design of an interactive robotic character using our soft skin modules on each of the robot’s links, pictured in Fig 1. These modules act as contact sensing bumpers, protecting both the human and the robot during interactions. The modules also include an underlying rigid frame which actuates the robot and provides structural support. 3D printed bearings are employed to reduce stress on the actuators during robot motion and physical interaction. The design of each module considers the range of motion for each joint, ensuring that target animated motions can be recreated. A major benefit of these 3D printed components is the ease by which they are reproduced and installed, making it simple to construct an interactive robot. In Section II of this paper, we discuss the considerations of animation

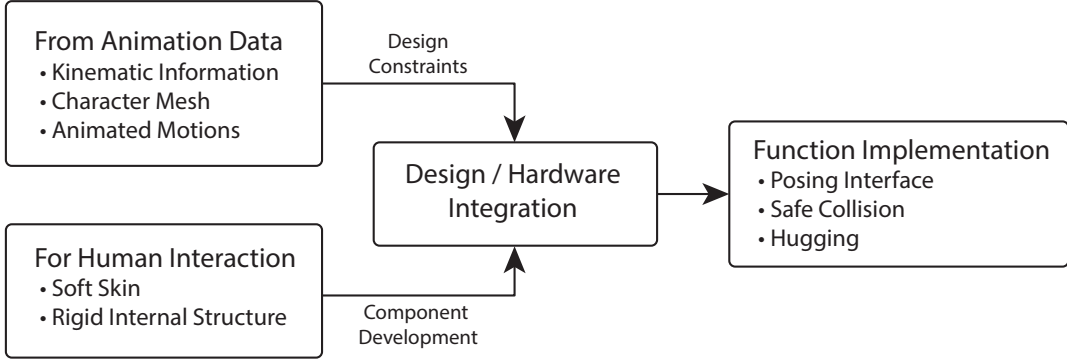


Fig. 2. Framework for designing mechanisms and interactive functions for a robot based on an animated character.

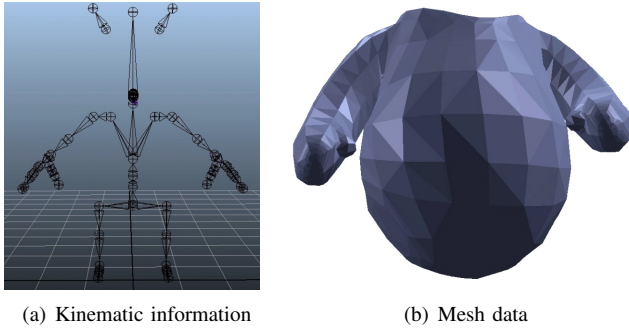


Fig. 3. Design driving features from the animation data include the kinematic structure and the mesh, or form, of the character.

data and physical interactivity in the design of our upper body robot. In Sections III and IV, we present the design and implementation of the 3D printed air-filled modules and the 3D printed bearings, respectively. Section V reports the implementation details and experimental results of an interactive “grab and move” interface for posing the robot. Our conclusions and future work are discussed in Section VI.

II. DESIGN CONSIDERATIONS

When designing a robot that will move and physically interact like an animated character, the kinematics and form of the character must be considered along with the necessity for durability and safety. The framework for designing the robot’s mechanisms and physical interactivity is shown in Fig. 2. This framework integrates the animated character data and the desired interactive functionalities to guide the development of a soft, modular robot that is safe, huggable and interactive.

A. Animation Data Constraints

The skeleton structure of an animated character is extracted from a given Maya model. As shown in Fig. 3(a), each arm in this model has four joints: two in the shoulder, one elbow joint, and one wrist joint. The torso has four serial vertebral joints with one end connected to the middle of the pelvis and the other end to the shoulder joints. There are also many joints in the hands. Further, every joint in the Maya rig has three degrees of freedom (DOF). It is impractical to

TABLE I
TARGET DIMENSIONS FROM MAYA AND ACTUAL LINK LENGTHS.

Dim.	Pelvis Width	Shoulder Width	Upper Arm	Forearm
Maya	20	22.96	9.82	6.96
Hardware	20	22.96	11.09	9.31

(unit: cm)

build hardware which has all of the DOFs of the animation model within the volume of the character shown in Fig. 3(b). Considering these factors, the robot hardware is designed to meet the following criteria:

- Number of DOFs is physically realizable.
- The hardware dimensions are close to those of the animated character.
- The range of motion allows its target motions to be realized.

For a robot which will focus on safe human-robot interactive motions like hugging, actuated hands are considered unnecessary. The arm configuration, which has a 3DOF shoulder joint and a 1DOF elbow joint, can perform grasping and hugging motions. The torso has a 2DOF pitch-yaw joint to make target motions such as crouching or arm swinging possible. In Table I, target lengths and corresponding hardware link lengths are shown. In our previous research [12], the width of the pelvis was fixed at 20cm. The lengths of the other links are determined by scaling the Maya model to match the pelvis width of 20cm. It should be noted that the forearm dimension from Maya is the length from the model’s elbow to its wrist. Due to the omission of wrist joints and actuated hands in our robot, the actual forearm length represents the distance from the elbow joint to the end of the hand.

B. For Physical Human Interaction

1) *Soft Skin*: Above all other design requirements is the requirement for safety. Presented in our previous study [11], a 3D printed soft skin module was developed which contains a flexible, contact-sensing air-filled cavity. This module helps to absorb unexpected impacts, reducing the likelihood of human injury and actuator damage. Further, the module provides contact force feedback via a pressure sensor



(a) Soft skin prototypes (b) Thrust bearing prototypes

Fig. 4. Initial prototypes of soft, air-filled contact sensors and rigid frame thrust bearing components

connected to the air-filled cavity. When distributed over the body of a humanoid, these modules give the robot the ability to sense contact forces on its various links. Full body sensing allows for the implementation of safe and engaging physical interactions. The independent sensing areas of the body allow a human to communicate with the robot through touch, drawing attention to certain links or guiding the motions of the robot. Prototypes for these air-filled, pressure sensing modules can be seen in Fig. 4(a).

2) Rigid Frame: An underlying support structure is necessary for a robot that will be lifted, played with and likely dropped. Underneath the soft skin, a rigid frame links the servos together. This frame also supports servo output shafts under loads experienced during motion and physical contact. In configurations where the servo's output shaft is especially vulnerable, modular 3D printed bearings are used to constrain motion and distribute loads. 3D printed thrust bearing prototypes are shown in Fig. 4(b).

III. AIR-FILLED LINKS

A humanoid upper body was designed and fabricated using 3D printed modular components and off-the-shelf sensors and servos. Considering various design constraints, a durable 10DOF robot was created with air-filled, contact sensing soft skin modules on its links. The robot has a 2DOF waist with pitch and yaw joints. The shoulder is 3DOF and the elbow is 1DOF. The range of motion for each joint and the mass of the body segments can be found in Table II. The total mass of the upper body is 2.2kg and the overall dimensions are $21.8 \times 31.0 \times 24.6\text{cm}$ ($H \times W \times D$). Detailed dimensions can be found in Fig. 5.

The 3D printed modules were created using a Stratasys Objet260 Connex multimaterial 3D printer [13], which can print a single part with both rigid and flexible features. The rigid materials used are VeroWhitePlus and VeroClear. The flexible rubber-like material is TangoPlus. The modules are designed to be assembled with Dynamixel MX-series servos [14].

The robot's upper body contains eight soft skin modules: one at each hand, one on each upper arm, two on the chest, one at the waist, and one on the back. These soft skin modules each include a soft, air-filled cavity. Each module's cavity is enclosed by a 1.5mm thick membrane of rubber-like material. The geometry of each module is

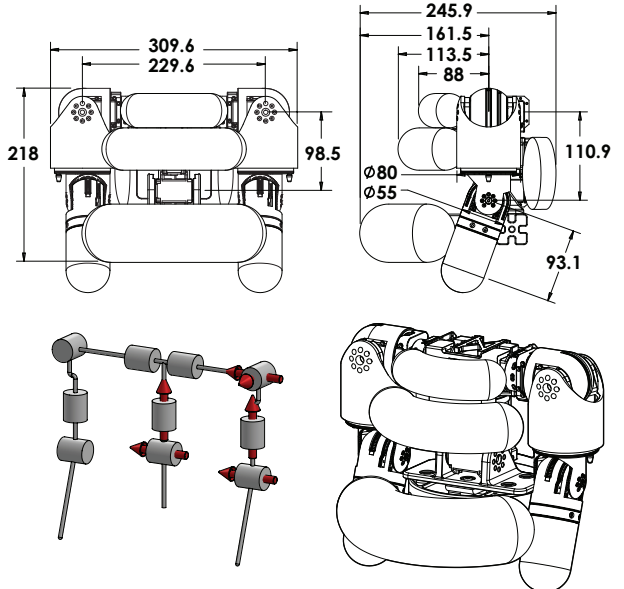


Fig. 5. Soft, toy sized humanoid upper body dimensions and kinematics

TABLE II
UPPER BODY SPECIFICATIONS

	DOF	Joint	Range of Motion	Mass (g)
Waist	2	Pitch	-3° to 28°	764.1
		Yaw	-85° to 85°	
Shoulder	3	Pitch	-180° to 180°	
		Roll	-95° to 70°	2 x 534.9
Elbow	1	Yaw	-90° to 90°	
		Pitch	-40° to 100°	2 x 185.3

cylindrical, hemispherical and/or toroidal in general because these flexible forms tend to auto-inflate after being deflated. Each module also consists of an inner rigid frame which provides structural support and servo mounting points.

At the end effector, or hand, of the humanoid is a module similar to our previous soft skin module. The cross section can be seen in Fig. 6(a). The module has been scaled down from the previous version to reduce mass and to fit within the given character mesh. The module is a 55mm diameter cylinder with a hemispherical tip that extends past the elbow joint by 120.5mm. Inside of the cavity is a rigid stick with a rubber-like ball on the end which prevents the module from being deflated to a shape from which it can not return. This module attaches directly to the end of a Dynamixel MX-28. On the servo-mounted end, where there is no room for air-filled features, a 3mm thick layer of rubber-like material is printed over the rigid frame. This use of soft material on segments where sensing does not occur can be seen throughout the robot's upper body helping to absorb impacts and providing a more consistent texture over the body.

A second soft skin module on the upper arm surrounds another MX-28 servo with an 80mm diameter cylindrical, air-filled cavity. Side view and top-down view cross sections of this model can be seen in Fig. 6(b). The servo is mounted inside of a rigid structural shell which doubles as the inner

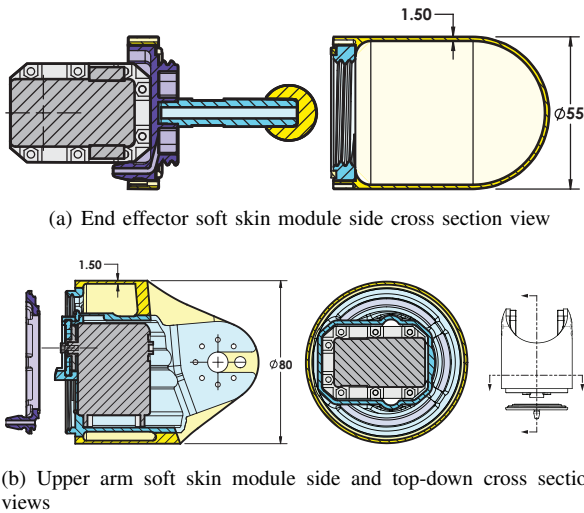


Fig. 6. Cross sections of the two soft skin threaded modules and caps for each arm. The flexible, rubber-like material is depicted in yellow and the rigid material in blue and purple; The rigid body of each module is blue and the caps are purple. The barbed fittings for connecting a tube and pressure sensor can be seen on each cap. The sections are cut mid-servo. All dimensions are in mm.

wall of the surrounding air-tight cavity. This rigid shell extends to the output of its parent actuator. The outermost wall of the cavity and its connections to the rigid inner wall are made of flexible material. As with the other soft skin modules, the membrane of this module is 1.5mm thick.

There are three independent semi-toroidal shaped soft skin modules on the front of the robot: two on the upper torso and one on the pelvis. Similar to the soft skin modules on the front of the robot, the air-filled module on the back senses contact from directly behind, as well as oblique rear angles. Where the character mesh leaves little room, a tall, shallow elliptical toroid segment provides a large sensing area within a shallow space.

Each module is printed with a standard 1/8" or 1/4" barbed tube fitting for repeated connecting and disconnecting of an air hose and pressure sensor. Each joint module also includes mechanical stops to limit the range of motion.

The method used to 3D print these soft skin modules, known as PolyJet printing, relies on a gel-like material to support overhanging part geometry as it prints each layer. This support material is UV-cured while printing, but can be broken up and removed post-print using a pressure washer. Cavities, therefore, must be printed with an opening through which this support material can be removed. A corresponding cap for each module is also printed to seal the cavity once clean.

The hand and upper-arm soft skin modules are sealed using threaded caps. A threaded module's main body and cap are each printed with o-ring like features which deform when tightened to create an airtight seal. On the torso, waist and back, where threaded caps can not fit, a simple cover is placed over the cavity opening and sealed using either epoxy or TangoPlus and left to cure under a high intensity UV light source.

IV. PRINTED BEARINGS

A. 3D Printed Thrust Bearing

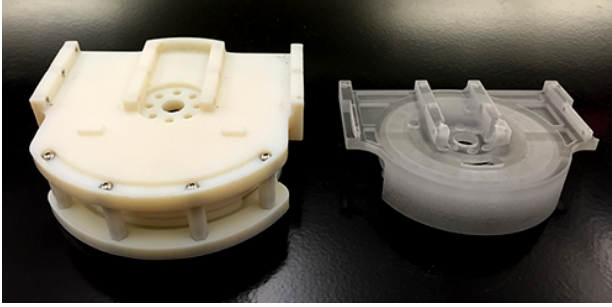
The robot's waist yaw joint is one of five joints where the link driven by the servo's output horn is unsupported by an idle horn on the opposite side of the servo. This leaves the servo's output shaft to bear the loads generated by robot motion and external forces. In these vulnerable locations, 3D printed bearings are employed to reduce the stress on the servo output shafts.

The waist yaw servo has an unsupported output shaft and heavy masses on either end of the joint. During motions like sitting and walking, or human interactions like being lifted, this joint's servo shaft will experience potentially damaging loads. A double direction tapered roller thrust bearing was implemented in the waist yaw joint because of its ability to withstand high axial tensile and compressive loads and impacts. The tapered roller bearing can also endure moments and radial loads.

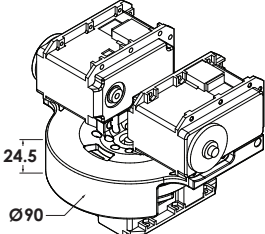
The first 3D printed thrust bearing experiments were performed with a simple tapered roller bearing model using multiple rigid materials, including VeroWhite, VeroClear and Digital ABS, with bearing races printed using both matte and glossy surface finishes. Examples of these test bearings are shown in Fig. 4(b). The harder VeroWhite and VeroClear materials allowed for much smoother rolling initially, and tended to get smoother as they were used and worn in over time. The rolling was smoothest when the bearing races were printed with a glossy surface finish. The roller assemblies were printed with a matte finish in each experiment so that the roller surfaces would have a consistent finish.

With this knowledge, the first double direction tapered roller bearing for the waist yaw joint was designed and fabricated. Seen in Fig. 7(a), this working prototype consists of upper and lower bearing race components which bolt together to sandwich two roller assemblies. The roller assemblies share an adjacent central component which provides the two inner bearing races and is fixed to the waist yaw servo body. The connected upper and lower bearing race components are directly driven by the yaw servo output shaft. Due to the eccentric location of the output axis on the servo case and the small desired diameter of the yaw bearing assembly, the bottom roller assembly can not form a complete circle and thus limits the range of motion of the waist yaw joint.

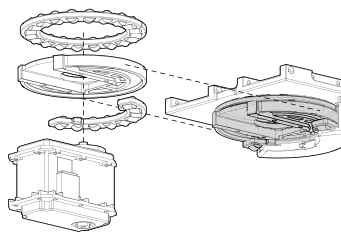
The final version of the double direction thrust bearing assembly, shown to the right of its predecessor in Fig. 7(a), is smaller and lighter than the previous version. The overall diameter of the bearing module is 90mm and the height is 24.5mm. These dimensions are shown in Fig. 7(b). The mass of the bearing is 102.6g, a 57% reduction from the previous version. While the size was reduced, the range of motion was increased from $\pm 61^\circ$ to $\pm 85^\circ$. The diameter of the assembly was reduced by combining the upper and lower bearing races into a single part, eliminating the need for hardware fasteners. The size of the conical rollers was reduced allowing room for more rollers. The upper roller



(a) Prototype (left) and final version (right)



(b) Bearing dimensions



(c) Bearing exploded view (shown from the rear)

Fig. 7. Waist double direction tapered roller thrust bearing prototype and final version. The exploded view includes the waist yaw servo, lower roller assembly, central bearing race component, upper roller assembly and the combined upper and lower bearing race component (from lower left, clockwise). All dimensions are in mm.

assembly has 20 rollers spaced 18° apart. The lower roller assembly, which is not a full circle, includes 9 rollers with the same 18° spacing. Adding more rollers further distributes loads and increases the operating smoothness of the bearing. An exploded view of the thrust bearing assembly can be seen in Fig. 7(c). Viewed from the lower rear, the diagram shows (from the lower left, clockwise) the waist yaw servo, lower roller assembly, central bearing race component, upper roller assembly and the combined upper and lower bearing race component. The upper and lower race component is driven by the servo output. The central race component is fixed to the yaw servo body.

As with the prototypes, the upper and lower roller assemblies are 3D printed as assembled parts and are unable to be disassembled. The bearing cage captures each roller in a conical cavity offset from the conical roller surface by 0.2mm . This clearance was determined by printing bearings with varying clearances and evaluating their ability to contain the rollers, ability to be printed reliably, ease of removing the initial support material and ability to roll smoothly. Rollers printed with a clearance larger than 0.3mm tend to fall out of the cage easily or jam. Rollers printed with less than 0.1mm clearance sometimes print fused to the bearing cage, unable to roll. When not fused, these small clearances create very narrow volumes of support material which are difficult access and break free by hand. Roller assembly clearances of 0.2mm are printed reliably, support material can be easily broken free by hand and washed away, and the rollers roll well within the cage.

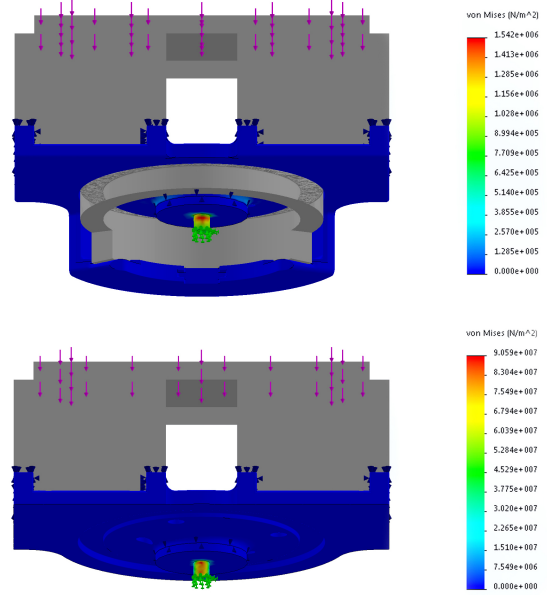


Fig. 8. Yaw servo shaft finite element stress analysis for a 50N compressive load with a double direction thrust bearing (top) and with no bearing (bottom)

After developing a satisfactory bearing module, friction was further reduced using a graphite-based, dry lubricant. The roller assemblies were coated with B'laster 8-GS Graphite Spray. For each application of the lubricant, the rollers were rotated in the cage to ensure a consistent coating around each of the roller's conical surfaces. The use of this dry lubricant reduces the friction within the roller assembly, and therefore reduces the friction between the servo and bearing module outputs.

B. Thrust Bearing Validation

TABLE III
SHAFT STRESS ANALYSIS WITH AND WITHOUT THRUST BEARING

Load Applied	Stress	Double Thrust Bearing	No Bearing
Tension (50N)	Avg.	$8.64\text{e}5$	$4.94\text{e}7$
	Max.	$1.54\text{e}6$	$9.95\text{e}7$
	Min.	$3.43\text{e}5$	$4.09\text{e}6$
Compression (50N)	Avg.	$8.64\text{e}5$	$4.49\text{e}7$
	Max.	$1.54\text{e}6$	$9.06\text{e}7$
	Min.	$3.43\text{e}5$	$3.77\text{e}6$

(unit: N/m^2)

The 3D printed bearing in the robot's waist yaw joint is a double direction tapered roller thrust bearing. Due to the offset location of the shoulder pitch motors, most forces experienced by the bearing produce a moment which causes the two bearings to share the load. The bearing assembly distributes these loads and moments down to the servo output shaft, as opposed to the servo output shaft.

Finite element analysis was used to validate the effect of the thrust bearing in reducing stress on the servo output shaft. A simplified loading simulation of the double direction thrust bearing was compared to a similar simulation without the

bearing. The stress simulation results are shown in Fig. 8 and Table III. With a fixed servo output shaft, the assembly was loaded using 50N compressive and tensile loads applied at the shoulder pitch servos. The configuration of these shoulder pitch servos on top of the waist yaw joint can be seen in Fig. 7(b). The force chosen represents twice the weight of the robot's upper body. In these two loading scenarios, the stress concentrations caused by sagittal bending can be seen on the front and back of the servo shaft. The double direction thrust bearing reduces the maximum stress in the shaft by distributing forces down to the rigid mounting flanges of the waist yaw servo case.

C. Friction Bearings

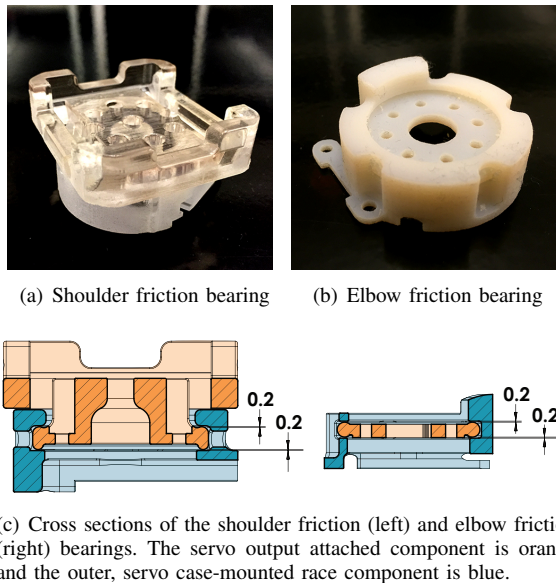


Fig. 9. Friction bearings are used to limit deflection in the shoulder and elbow joints where a thrust bearing can not fit. The clearance between the inner and outer components is 0.2mm.

There are four other servo output shafts with no supporting idle horns: one at each shoulder and one at each elbow. In these small spaces, where a roller bearing can not fit, friction bearings, shown in Fig. 9(a) and 9(b), are used to limit stress on the servo output shafts. The role of the friction bearing is to support the servo output shaft when loaded to prevent excessive deflection and stress. Each friction bearing consists of two parts. The inner component of the bearing, which includes a disk that attaches directly to the servo horn, is captured by the outer component of the bearing. The inner and outer components are shown in orange and blue, respectively, in Fig. 9(c). The outer component attaches directly to servo's case, providing two rigidly supported bearing surfaces. For rigidity and compactness, these two components are printed as one assembled module which cannot be disassembled.

Under normal loading, the inner disk component of the friction bearing is in its neutral position and does not contact the bearing surfaces. In this neutral configuration, a 0.2mm

clearance exists in the axial direction between the inner disk's toroidal edge and each of the outer component's bearing surfaces. Only when the servo shaft is deflecting do these bearing components make contact. When a joint experiences a force or moment large enough to deflect to the limit, the joint may still operate, albeit with increased rotational friction. These modules do not protect against loads applied perpendicularly to the servo shaft.

V. INTERACTIVE FUNCTION IMPLEMENTATION

Fig. 10 shows a series of snapshots of our experiment. Each air-filled link on the robot is a soft skin module connected to a pressure sensor using a flexible tube. The module is sealed and holds its shape when connected. The pressure sensors are connected to the A/D channels of the servo motor controller board. The pressure sensor used is a MPX5500DP Freescale air pressure sensor. The controller is an OpenCM9.04 board with an OpenCM485EXP expansion board [15]. Control commands are sent to the servos every 10ms using TTL (Transistor-transistor Logic).

A simple user interface for human-robot interaction is implemented in the control system to verify the hardware. The interface provides "grab and move" functionality for easily posing the robot. In this function, desired joint angles are the angles measured in the previous control period. The joint controller holds the servo motor for a given link at its desired angle while the pressure of its corresponding soft skin module (P_i) is less than a threshold pressure ($P_{threshold}$). If P_i becomes larger than $P_{threshold}$, the parent joint is made powerless by the joint controller. An experiment using this function is depicted in Fig. 10. In Fig. 10(a), the robot's left forearm is grabbed by a human causing the left elbow joint to become powerless and move freely. Fig. 10(b), 10(c), 10(d) and 10(e) show that the implemented function works for posing each of the air-filled links. In Fig. 10(f), the robot maintains the final pose created by physical interaction with a human.

VI. CONCLUSION AND FUTURE WORK

The design considerations and hardware implementation for an upper body robot for physical human-robot interaction are presented in this work. This upper body has 10 actuated DOFs. Its arms, pelvis, chest and back have soft, 3D printed, air-filled modules connected to pressure sensors to provide contact sensing and safe interaction. These soft skin modules cover the underlying actuators and the rigid 3D printed frame with printed bearings. We validated the effect of our bearing design using simulation and showed experimentally that the developed upper body system is capable of physical interaction.

To further optimize the design of this robot, it will be necessary to better understand the mechanical properties of the various 3D printable materials. Knowledge of such properties will allow us to drive down the mass of the components with confidence that parts will not fail while moving or interacting. A better understanding of the flexible material properties will allow us to push towards more soft,

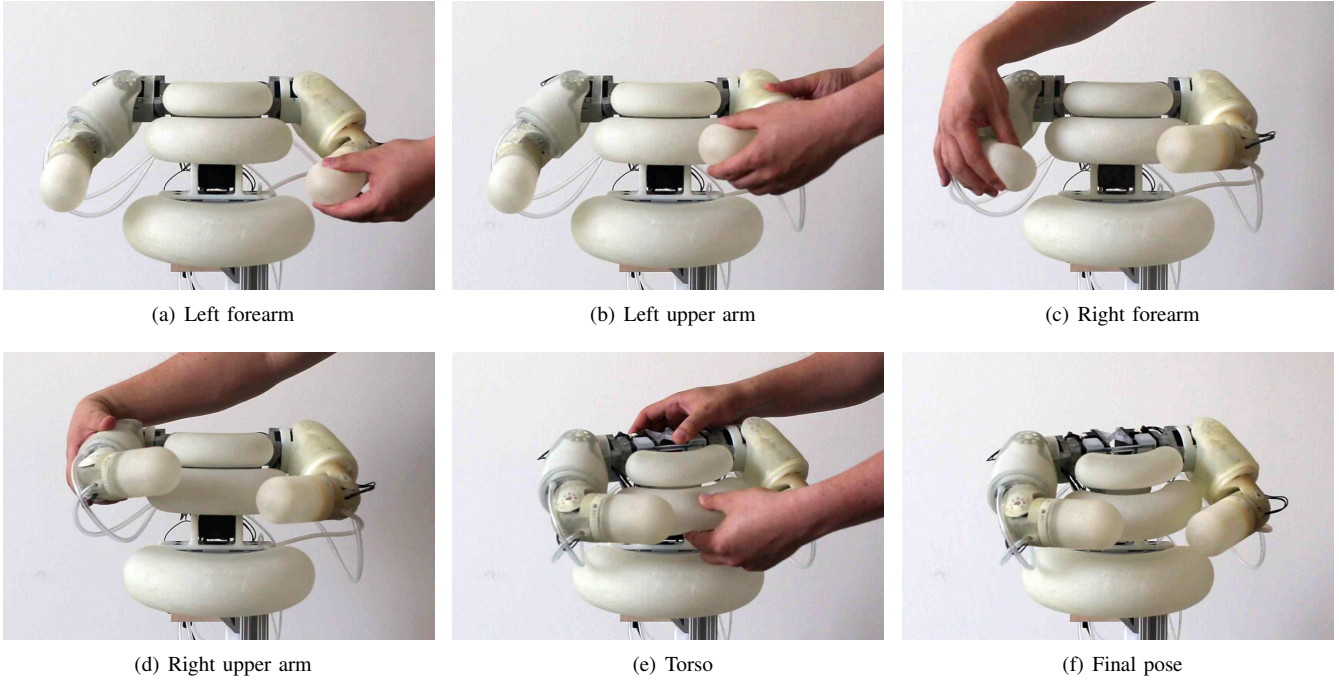


Fig. 10. Posing the upper body by grasping and moving each air-filled link

durable and complex designs with more sensing capabilities. Components like the 3D printed bearings should be tested to determine how and when they will wear out, as well as how much load they can support.

Currently the soft skin modules can roughly sense the magnitude of a contact force, but can not sense the location or direction. We will continue to explore other soft skin module designs that allow these contact force details to be sensed. Further, we will develop more reliable methods for sealing the air-filled cavities without sealant.

We plan to continue the development of human-robot interactive functions using this upper body. Some candidate functionalities are physically interactive motions such as hugging, learning by demonstration and gently grasping or holding objects. To implement these functions, it will be helpful to know more about a human's physical capabilities (gripping power, etc.). Further, collaboration with psychologists will be worthwhile in researching a human's mental state while interacting with this robot character. This upper body will be attached to the lower body from our previous study for whole body motion and physical interaction.

REFERENCES

- [1] Aldebaran. (2014) Who is Pepper? [Online]. Available: www.aldebaran.com/en/a-robots/who-is-pepper
- [2] Y. Sakagami, R. Watanabe, C. Aoyama, S. Matsunaga, N. Higaki, and K. Fujimura, "The intelligent ASIMO: System overview and integration," in *Intelligent Robots and Systems, 2002. IEEE/RSJ International Conference on*, vol. 3. IEEE, 2002, pp. 2478–2483.
- [3] M. Fujita, Y. Kuroki, T. Ishida, and T. Doi, "Autonomous behavior control architecture of entertainment humanoid robot SDR-4X," in *Intelligent Robots and Systems, 2003. (IROS 2003). Proceedings. 2003 IEEE/RSJ International Conference on*, vol. 1, Oct 2003, pp. 960–967 vol.1.
- [4] I. Ha, Y. Tamura, H. Asama, J. Han, and D. W. Hong, "Development of open humanoid platform DARwIn-OP," in *SICE Annual Conference (SICE), 2011 Proceedings of*. IEEE, 2011, pp. 2178–2181.
- [5] Aldebaran. (2014) Who is NAO? [Online]. Available: [https://www.aldebaran.com/en/humanoid-robot/nao-robot](http://www.aldebaran.com/en/humanoid-robot/nao-robot)
- [6] K. Wada, T. Shibata, T. Masha, and S. Kimura, "Robot therapy for elders affected by dementia," *Engineering in Medicine and Biology Magazine, IEEE*, vol. 27, no. 4, pp. 53–60, July 2008.
- [7] C. Fitzgerald, "Developing Baxter," in *Technologies for Practical Robot Applications (TePRA), 2013 IEEE International Conference on*, April 2013, pp. 1–6.
- [8] W. Stiehl, J. Lieberman, C. Breazeal, L. Basel, L. Lalla, and M. Wolf, "Design of a therapeutic robotic companion for relational, affective touch," in *Robot and Human Interactive Communication, 2005. ROMAN 2005. IEEE International Workshop on*, Aug 2005, pp. 408–415.
- [9] K. Kobayashi, T. Yoshikai, and M. Inaba, "Development of humanoid with distributed soft flesh and shock-resistive joint mechanism for self-protective behaviors in impact from falling down," in *Robotics and Biomimetics (ROBIO), 2011 IEEE International Conference on*, Dec 2011, pp. 2390–2396.
- [10] T. Minato, Y. Yoshikawa, T. Noda, S. Ikemoto, H. Ishiguro, and M. Asada, "CB2: A child robot with biomimetic body for cognitive developmental robotics," in *Humanoid Robots, 2007 7th IEEE-RAS International Conference on*, Nov 2007, pp. 557–562.
- [11] J. Kim, A. Alspach, and K. Yamane, "3d printed soft skin for safe human-robot interaction," in *Intelligent Robots and Systems (IROS), 2015 IEEE/RSJ International Conference on*, accepted.
- [12] S. Song, J. Kim, and K. Yamane, "Development of a bipedal robot that walks like an animation character," in *Robotics and Automation, 2015. ICRA '15. IEEE International Conference on*, June 2015.
- [13] Stratasys. (2014) Object260 connex. [Online]. Available: <http://www.stratasys.com/3d-printers/design-series/object260-connex>
- [14] Robotis. (2014) Mx-series e-manual. [Online]. Available: http://support.robotis.com/en/product/dynamixel/dxl_mx_main.htm
- [15] —. (2014) Opencm9.04 e-manual. [Online]. Available: <http://support.robotis.com/en/product/auxdevice/controller/opencm9.04.htm>